



Title	Transient Arc Diagnosis with OMA(Welding Physics, Processes & Instruments)
Author(s)	Arata, Yoshiaki; Miyake, Shoji; Yoshioka, Yasuo et al.
Citation	Transactions of JWRI. 1980, 9(1), p. 47-51
Version Type	VoR
URL	https://doi.org/10.18910/7080
rights	
Note	

The University of Osaka Institutional Knowledge Archive : OUKA

<https://ir.library.osaka-u.ac.jp/>

The University of Osaka

Transient Arc Diagnosis with OMA[†]

Yoshiaki ARATA*, Shoji MIYAKE**, Yasuo YOSHIOKA*** and Hidesato MATSUOKA***

Abstract

Spectroscopic study of a pulsed high current arc was performed with efficient usage of optical multichannel analyzer (OMA). Not only spectral line profiles but also their spatial distributions could be detected quite easily shot by shot. But at the gate mode operation of OMA, it is demonstrated that much care should be taken in the selection of pulse waveform as well as its height for the correct profile measurement.

KEY WORDS: (Transient Arc) (Spectroscopy) (OMA) (Spectral Line Profile) (Spatial Distribution)

1. Introduction

In the spectroscopy of emitted light from many kinds of radiation sources, a photomultiplier has been most frequently used as an electrical detector of photon signals. However when an emitter is a pulse source and has a strong shot by shot variation, it is difficult to obtain correct and reliable informations by using one photomultiplier. Sometimes multichannel photomultipliers are applied to avoid this difficulty in conjunction with optical fiber system, but it is very complex and a spatial or wavelength resolution is not so good usually.

To solve these problems spectroscopic measurement by using vidicon or image sensor has attracted much attention in these days. It has given satisfactory results in chemical research, for instance, but in the field of plasma physics and/or discharge they began to use¹⁻³⁾ this type of a detector quite recently. We also studied⁴⁾ already a pulsed high current arc by using an optical multichannel analyzer (OMA) of PAR. In our opinion it is very important and favorable to apply this diagnostic method for welding research : for instance the detailed study of many kinds of arc heat sources, weld pool behaviours emitting different optical signals, and imaging of the dynamic behaviours of EB welding and so on.

We give in this paper some experimental results based on the application of OMA for the spectroscopic study of a transient arc⁴⁾ we have developed. Various important problems are discussed for the correct measurement with OMA and its utilities are also demonstrated by experimental data.

2. Experimental Apparatus

2.1 OMA system

The OMA we use is composed of console (PAR, Model 1205A), SIT detector (PAR, Model 1205D) and a gate pulser. The cross section of a SIT detector is shown in Fig. 1. Optical signals passing through a monochromator are amplified by image intensifier and stored on silicon

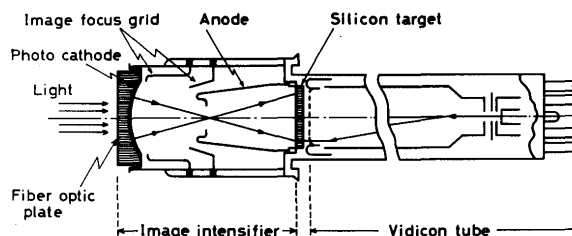


Fig. 1 Cross section of silicon intensified target (SIT) detector (1205 D).

target. Vidicon enables us to make data processing of the stored signal with the console. The dimension of the silicon target to be able to receive a signal is 12.5 mm in length and 2.5 mm in width. It is channeled in length by 500 areas with 50% MTF resolution limit of 14 lp/mm. In case of wavelength scanning of an optical signal, 500 channels are lined up in the wavelength direction of a monochromator exit. So that wavelength resolution is essentially limited by the inverse dispersion of a monochromator. While when we want to know a spatial distribution of a selected spectral line, we first focus the plasma image on the entrance slit of the monochromator

[†] Received on April 5, 1980

* Professor

** Associate Professor

*** Graduate Student

so as to the lateral direction of the plasma is parallel to the slit. By making 500 channels to be distributed parallel to the slit image at the outlet of the monochromator, we easily obtain a spatial distribution of the plasma. In this case, however, we must notice that total intensity of a line can be measured only when it is widened below 2.5 mm on the detector surface.

In a transient spectroscopy we use a gate pulser. At the real time operation the image intensifier is biased negatively to -9.0 kV. At the gate mode operation the negative bias is lowered to -7.5 kV. It makes the gating on-off ratio to be $10^4:1$. A high voltage pulse up to -1.5 kV is applied to image focus grid in Fig. 1. The waveform and the pulse intensity affect the focusing characteristics and PAR recommends to give the gating voltage $|V_g| \geq 1.2$ kV.

2.2 Plasma source

Figure 2 shows the schematic diagram of plasma apparatus⁴⁾. A gas circulating system once evacuated below

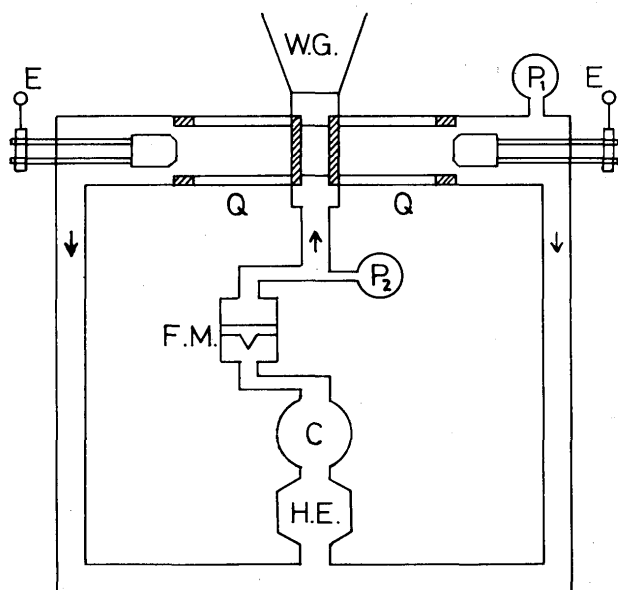


Fig. 2 Schematic diagram of plasma apparatus.

1×10^{-2} Torr is filled with He and H_2 gas mixture at atmospheric pressure. The compressor C gives the vortex gas flow ($\phi \leq 1800$ l/min) from the center in a quartz pipe Q of 40 mm in diameter. The initial plasma is produced by a CW microwave ($P_i \leq 80$ kW, $f = 906$ MHz) through the waveguide WG. Dimensions of this plasma vary with external parameters but typically they are 20 – 30 cm in length and 2 – 6 mm in diameter. For the high current arc formation two electrodes E are inserted axially with the inter-electrode distance of 24 cm, satisfying a good contact with the initial plasma.

2.3 Diagnostic system

Spectroscopic observation is performed side-on to the central region of the arc as shown in Fig. 3. The $V_p - I_p$ characteristics is displayed to a synchroscope by a divider and a Rogowsky coil. The main discharge is triggered from OMA console to a condenser bank ($100 \mu F$, 10 kV). Two 1-m monochromators (Mizojiri) are used with the inverse dispersions of 8.0 A/min and 4.8 A/min. Also a standard lamp (Eppley, Type-EP) is used for the calibration of a monochromator and detector system.

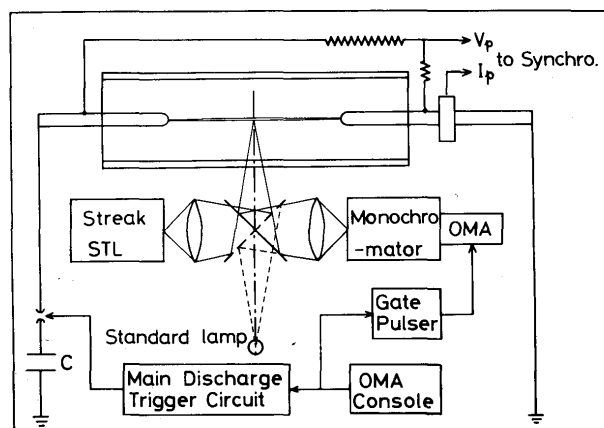


Fig. 3 Block diagram of diagnostic system.

3. Results and discussions

Before spectroscopic observation of the arc plasma, we've made several calibrations of the SIT detector. First the instrumental width was checked by using He-Ne laser ($\lambda = 6328 \text{ \AA}$). In Fig. 4a) the optical signals are displayed for real time and gate operations of the detector. At the real time operation the halfwidth is only 2 channels but in the gate mode it is widened to 4 channels. These widths are, of course, very small and negligible compared with those of several lines under study. In Fig. 4b) an example is given of the wavelength dispersion of HeII 4686 line from the pulsed arc. It shows a typical Stark profile and its halfwidth is much larger than the instrumental one in Fig. 4 a). Also is shown on the left side of Fig. 4 b) an example of lateral distribution of HeII 4686. Since the spectral halfwidth of the line is about 1.2 mm in length on the detector surface, this spatial profile corresponds to the total intensity distribution of the line. A good transient spatial profile of the emitted photons is thus obtained successfully.

As for the uniformity of the optical response of the detector along channels, we checked it by scanning the laser light on the monochromator and confirmed the flatness of the response for both real time and gate operations.

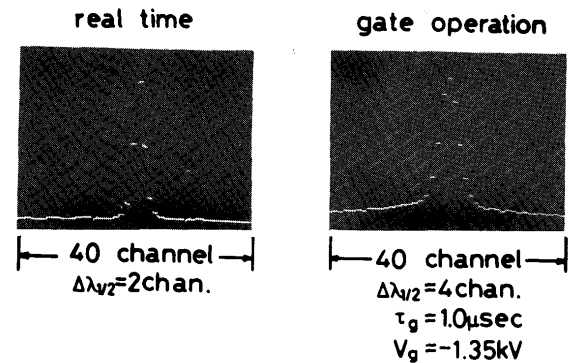
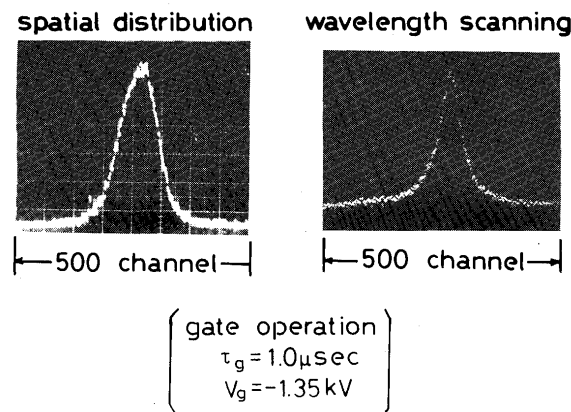
a) calibration $\lambda = 6328 \text{ \AA}$ (He-Ne laser)b) He II 4686 \AA (plasma)

Fig. 4 Calibration signals of the detector and examples of a line profile and a spatial distribution of HeII 4686 under study.

Figure 5 shows examples of OMA signals with the wavelength dispersion. In the middle of the upper part of the traces is also shown $V_p - I_p$ characteristics. Stark broadened profiles of various lines are given in the central and the lower parts, from which we can decide electron density n_e . The electron temperature T_e is calculated from the total intensity ratio of HeII 4686 and HeI 5876 with CR model.

While a time development of HeII 4686 spatial distribution at $P_i = 20 \text{ kW}$ is shown in Fig. 6. As is clearly seen the ion line begins to emit steeply at $t \gtrsim 6 \mu\text{S}$ and after $t \gtrsim 10 \mu\text{S}$ strong deformation occurs owing to the growth of helical instability. Meanwhile at $P_i = 40 \text{ kW}$ a slower increase of the ion line is observed and the instability growth is delayed to $t \gtrsim 13 \mu\text{S}$. Since the increase in P_i brings forth that of the initial plasma diameter, a larger microwave reduces the current density of the pulsed arc and less heating is observed with a better stability.

We can thus measure quite easily emitted optical intensity profiles with a good S/N ratio. An instant measurement of a spectral line profile is convenient to obtain

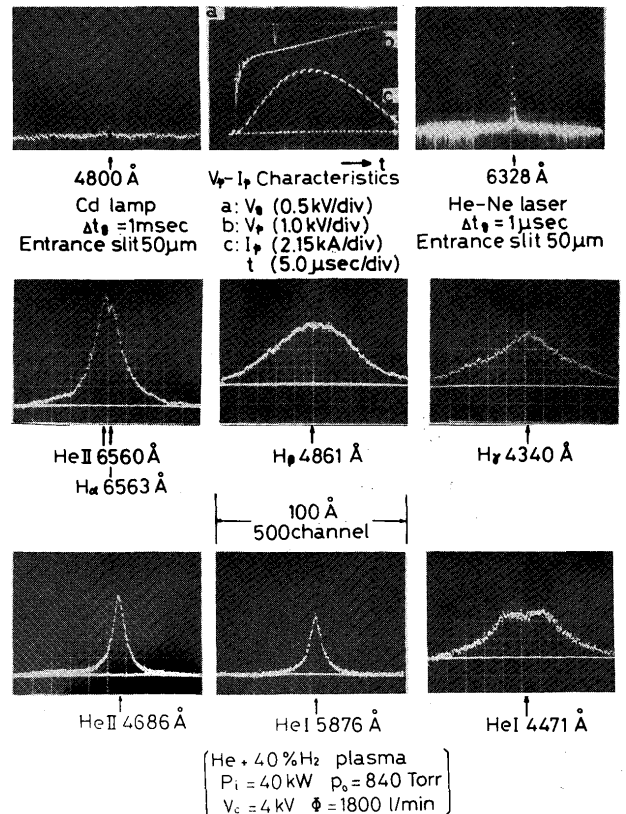


Fig. 5 OMA signals for various spectral lines from the arc column. Also shown is $V_p - I_p$ characteristics and the calibration lines.

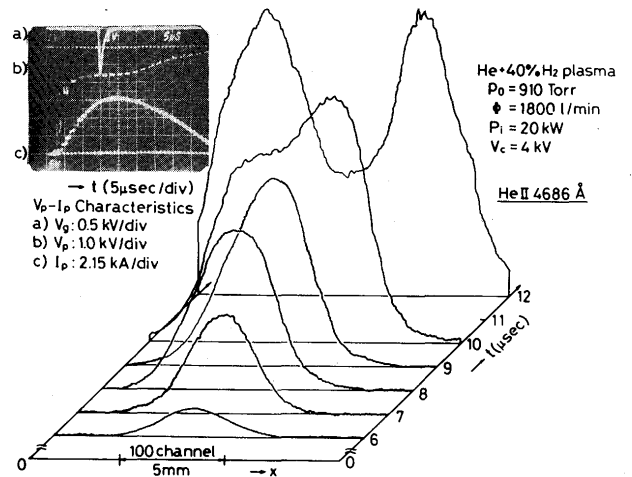


Fig. 6 Example of a time development in the spatial distribution of HeII 4686 during high current supply.

total intensity and line width. It offers a prompt decision of plasma parameters (n_e , T_e etc). While instant data acquisition of a spatial distribution enables us to study the stability of a plasma in detail. These superiorities come from the fact that the SIT detector can be operated at the gated mode. But in the following we remark that besides the gating voltage, the pulse waveform has a sub-

stantial effect on both spatial and spectral profiles.

By an appropriate selection of external parameters we can obtain a stable and radially symmetric arc column with a good reproducibility. At such a parameter we have performed shot by shot measurement of HeII 4686 line profile as shown in Fig. 7. In this figure data for two types of pulse waveform (see the right side of the figure) are given. In case of a nearly rectangular waveform (the upper part) almost symmetric line profiles are obtained even when the line center is shifted along channels. But in case of a bad waveform as in the lower part, strongly asymmetric profiles appear by the shifting of the line center, even though V_g is greater than that of the upper case. These asymmetries are also observed in the instant spatial distribution measurement. This feature is not observed clearly when we use a thin line from He-Ne laser or discharge lamps. Figure 8 shows the effect of V_g variation on the line profile. Here the line center is shifted to

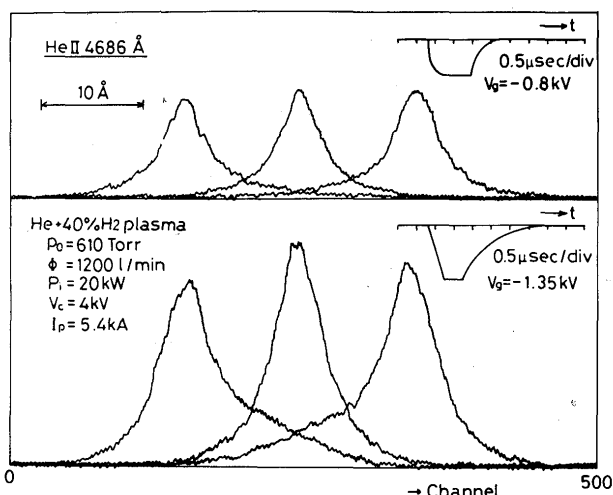


Fig. 7 HeII 4686 line profiles for two waveforms of the gate pulse.

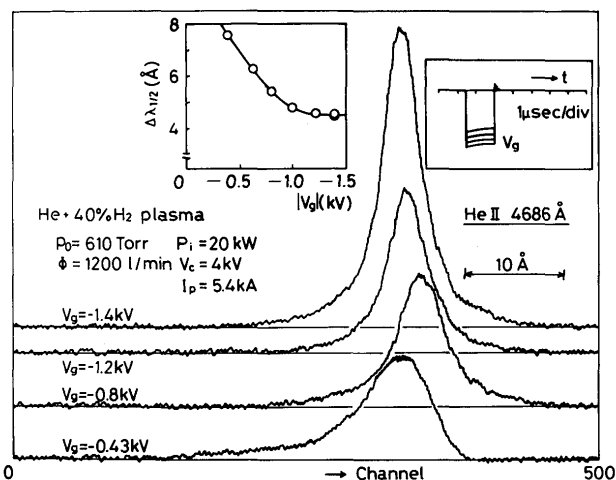


Fig. 8 HeII 4686 line profiles for different gating voltages.

the right for us to be able to find the asymmetry more clearly. The gating pulse waveform is accurately rectangular as shown on the upper right side. With the increase in $|V_g|$ asymmetry in the line profile is improved and its halfwidth $\Delta\lambda_{1/2}$ is lowered (see the upper left side). At $|V_g| > 1.3 \text{ kV}$ $\Delta\lambda_{1/2}$ becomes nearly constant. This nature is also noticed by PAR but no information as to its asymmetry. When we see the configuration of the detector in Fig. 1 these problems can be understood as the result of defocusing in the image intensifier, because at the real time operation (-9.0 kV DC bias to the intensifier) electrons from photocathode is designed to focus most effectively and enter on to the target satisfying a faithful correspondence between photon distribution and electrons' one. Thus we may say that a pulser must be used which generates an exactly rectangular waveform of -1.5 kV . Of course when, different from our source, the photon emission from a source is shorter than the gating time duration, only pulse intensity affects the detector quality.

Figure 9 shows an example of the temporal change of electron temperature for various microwave powers. As

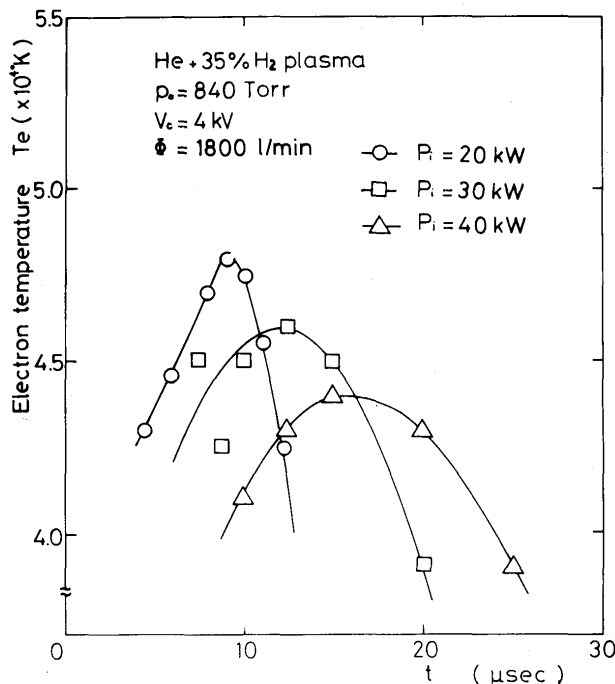


Fig. 9 Example of temporal changes of electron temperature averaged in the radial direction for various microwave powers.

stated earlier a higher microwave power brings about a moderate heating. So that it is clearly seen that the heating rate is larger with a higher peak temperature for $P_i = 20 \text{ kW}$ as compared with 30 or 40 kW. Figure 10 is an example of the radial distribution of n_e and T_e . We see $T_e \approx 5 \times 10^4 \text{ K}$ and $n_e \lesssim 1 \times 10^{17} \text{ cm}^{-3}$. These values are

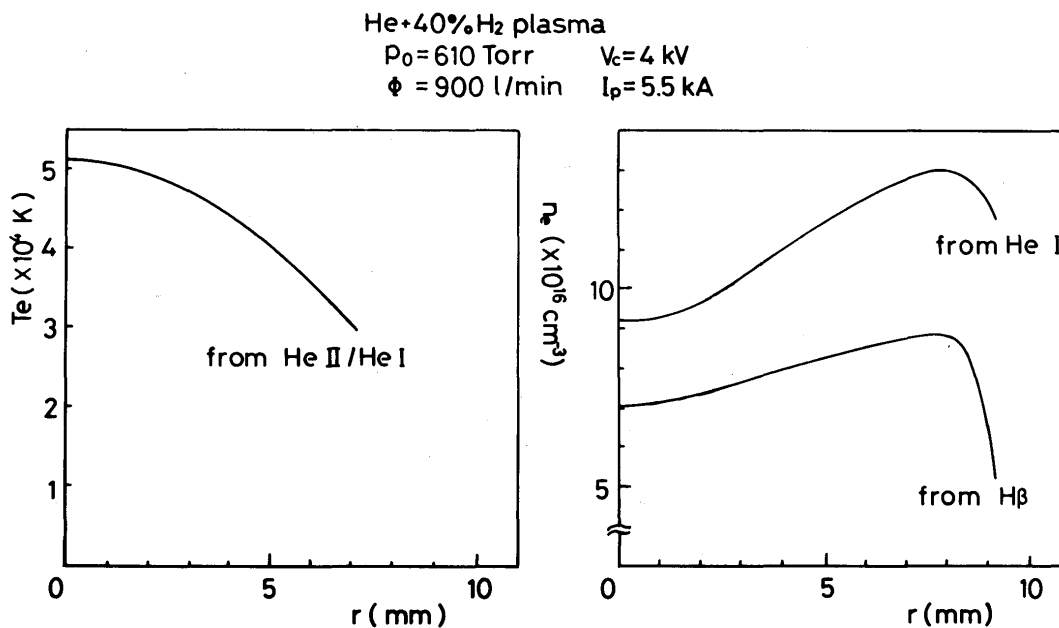


Fig. 10 Example of radial distributions of electron temperature and electron density.

typical for this pulsed arc and different values in n_e can be obtained easily by varying the filling pressure.

4. Conclusion

By using optical multichannel analyzer (OMA) system a pulsed high current arc was studied experimentally. For each discharge shot a spectral line profile and /or its spatial distribution could be detected with a good time resolution and fine S/N ratio. Plasma parameters (n_e , T_e) and the correlation between heating efficiency and instability growth could thus be decided quite easily. After some calibrations for the OMA detection, it was demon-

strated that the pulse waveform has substantial effect on the correct profile measurement at the gate mode operation.

References

- 1) M. E. Bacon, A. J. Barnard and F. L. Curzon: J. Quant. spectrosc. Rad. Transfer 18 (1977) 3999.
- 2) W. T. Chiang and H. R. Griem: Phys. Rev. A18 (1978) 1169.
- 3) R. Pal and H. R. Griem: Phys. of Fluids 22 (1979) 1790.
- 4) Y. Arata, S. Miyake, M. Ushio and Y. Yoshioka: J. Phys. Soc. Japan 44 (1978) 1483.